3873

LOW-PROFILE, WIDE-BAND ANTENNAS FOR WIRELESS COMMUNICATIONS

A THESIS SUBMITTED TO THE GRADUATE DIVISION OF THE
UNIVERSITY OF HAWAI'I IN PARTIAL FULFILLMENT
OF THE REQUIREMENTS FOR THE DEGREE OF

MASTER OF SCIENCE

IN

ELECTRICAL ENGINEERING

AUGUST 2004

By
Jodie M. Bell

Thesis Committee:

Magdy F. Iskander, Chairperson
Wayne A. Shiroma
M. Fatih Demirkol
Zhengqing Yun

TABLE OF CONTENTS

ABSTRACT

This thesis presents the implementation of electromagnetic band-gap (EBG) structures with an inherently wide-band Archimedean spiral antenna. The EBG structure is designed to emulate a perfect magnetic conductor (PMC). This combination provides a highly desirable low-profile and wide-band antenna. Utilization of an EBG structure offers an antenna height reduction of 92% compared to the traditional $\lambda/4$ cavity backed implementation of spiral antennas. This design also offers full scalability and the implemented approach allows the spiral antenna to maintain a considerable fraction (71%) of its designed inherent broadband characteristics with no reduction in gain.

LIST OF FIGURES

LIST OF SYMBOLS

λ	Wavelength
Z	Impedance
E	Electric Field
H	Magnetic Field
a	Period
h	Height
w	Width
d	Depth or Diameter
η	Intrinsic Impedance
k	Wave Vector
μ	Magnetic Permeability
ε	Electric Permittivity
ω	Frequency (radians per second)
c	Speed of Light in a Vacuum or Circumference
s	Spacing
t	Thickness
L	Inductance
C	Capacitance
$B.W.$	Bandwidth
l	Length
ϕ	Polar Angle
r	Radius

CHAPTER 1: INTRODUCTION

Today's wireless revolution is constantly demanding that communications technologies cover additional access and broader applications while continuing to use compact and low-cost devices. Whether the applications are military or commercial, with the complexity of wireless communications technologies and the numerous elements required for these technologies, available device size has become a highly valued commodity. To more efficiently use the available space offered within these devices, engineers are using fewer and more compact antennas. A possible procedure for achieving this is by designing compact, broadband antennas that cover a wide range of applications. With the current trend of wireless technology innovation there is a vast array of wireless applications but few low-profile, wide-band antenna designs. Many of these applications, ranging from space to shipboard applications, need antennas that are low-cost, compact, and broadband.

Spiral antennas have characteristics that are vital for a wide range of wireless applications. They are inherently wide-band antennas with relatively low profiles that are simple and of low cost to manufacture. These characteristics make spiral antennas prime candidates for sensor type applications on airborne, ground-based, mobile, shipboard, and space platforms.

Traditional implementation of Archimedean spiral antennas entails using a perfect electric conducting (PEC) ground plane at a distance of $\lambda/4$ below the antenna to produce a unidirectional beam. This implementation is commonly constructed by backing the spiral with a metallic cavity, creating a cavity-backed Archimedean spiral

antenna. This approach introduces a fixed physical length between the antenna and the ground plane in terms of λ, thus, increasing the size, particularly at lower frequencies, and limiting the antenna's frequency independent characteristics. In an effort to correct this problem it is common to load the cavity with absorbing material to reduce the resonance effects. However, this is done at the cost of antenna performance, specifically, a 3dB loss in gain [1, 2]. The objective of this thesis work is to overcome these limiting effects by introducing the novel implementation of an Archimedean spiral antenna backed by an electromagnetic band-gap (EBG) structure.

As mentioned earlier, a PEC ground plane acts as a good reflector to produce a unidirectional beam in the traditional implementation. However, there are various reasons why it is not effective to use a PEC ground plane with an antenna that is excited by electric current. Image theory states that for electrically excited antennas, a PEC ground plane will produce an image with currents opposite of those in the antenna [3]. When these reverse image currents are brought too close to the antenna they will effectively short circuit the antenna. Additionally, at close distances between the antenna and the ground plane, the fields reflected by the PEC ground plane (or its image) will be almost 180° out of phase of the incident fields [4]. This phase offset can cause destructive interference with the incident waves and, hence, seriously limit the amount of radiated power. Extended PEC ground planes also support propagating surface-waves [5]. These propagating surface-waves can radiate into space and produce undesirable interference with the antenna radiation. It is for these reasons that electrically excited antennas are traditionally backed by $\lambda/4$

cavities. This traditional implementation is done to counteract the 180° phase change as well as to reduce the undesirable interactions produced by the reverse image currents and propagating surface-waves.

Alternatives to the traditional implementation of electrically excited antennas and PECs have been developed to reduce the undesirable results of this implementation. One alternative is to alter the antenna design without altering the ground plane design. Rather than implementing an electrically excited antenna, research has been done to develop antenna designs (slot antenna elements) that are excited by an equivalent magnetic current. Therefore, allowing the PEC ground plane to produce an image with currents in the same direction as those in the antenna [3]. This implementation may, however, introduce complicated feed structures. Another approach is to alter the ground plane design without altering the antenna design. Theoretically, rather than implementing a PEC ground plane, it wound be optimal to back an electrically excited antenna with a perfect magnetic conducting (PMC) ground plane. A PMC ground plane would produce, for an electrically excited antenna, an image with currents in the same direction as the currents in the antenna [3]. The use of a PMC ground plane would also eliminate the 180° phase offset induced by a PEC ground plane [6]. Additionally, the implementation of a PMC ground plane would suppress propagating surface-waves [5]. Implementation of a PMC ground plane will allow significant reduction in profile without reduction in antenna performance. However, no PMC exists in nature, therefore, to produce the

desired effects, EBG structures are being designed as a realizable alternative to a PMC.

Chapter 2 begins this work with a description of the limitations of PEC ground planes, followed by the introduction of possible design alternatives. This is followed, in Chapter 2, with a background presentation of high-impedance EBG structures, their advantages, and their design. Beginning in Chapter 3, an EBG structure is initially designed for the simple case of a $\lambda/2$ dipole. Continuing through Chapter 3, the success of this design to function as an efficient ground plane is validated through antenna simulation and evaluation of the performance when placed above the EBG structure. After the combined implementation of the EBG structure and dipole design is tested and validated, a review of Archimedean spiral antennas, their attributes, and their design procedure is given in the beginning of Chapter 4. Continuing in Chapter 4, an Archimedean spiral antenna is designed for the desired frequency range of 8-16GHz and is implemented with the designed EBG structure to create a novel low-profile and wide-band antenna. As it may be seen in Chapter 4, to test the effectiveness and the advantages of backing a wide-band antenna with an EBG structure, various analyses are conducted on the design's performance. These analyses show the effectiveness of this novel implementation to provide a high-performance, low-cost, low-profile, wide-band antenna. In Chapter 5 the scalability of the designed EBG structure is tested and validated with the case of a $\lambda/2$ dipole and with the case of an Archimedean spiral antenna. Finally, in Chapter 6 the work is summarized and proposed future work is discussed.

CHAPTER 2: ELECTROMAGNETIC BAND-GAP STRUCTURES

As mentioned earlier, implementing PECs with electrically excited antennas comes with limitations. This chapter begins with a detailed discussion of these limitations. This discussion is followed by a presentation of alternative designs to the traditional implementation of electrically excited antennas and PECs. Next, a detailed description of high-impedance EBG structures and their design is given. As will be discussed, EBG structures can be designed to emulate PMCs, which when implemented in antenna designs can provide significant advantages.

2.1: Limitations of PEC Ground Planes

Backing an electrically excited antenna with a PEC ground plane does offer a good reflector for producing a unidirectional radiation pattern. However, PEC ground planes have very low surface impedances. These low impedances result in a very low ratio of electric fields to magnetic fields. Therefore, there are zero tangential electric field components at the surface (E-Field node) and double tangential magnetic field components at the surface (H-Field anti-node). Because of the low impedances, PECs have properties undesirable for implementation as ground planes for electrically excited antennas. These properties include reverse image currents, 180° phase shift of reflected waves, and unsuppressed propagating surface-waves [3, 4, 5]. To implement PEC ground planes, precautions need to be taken to minimize the effects of these properties. Traditionally the antenna is placed at a distance of $\lambda/4$ above the PEC ground plane. This distance allows the 180° phase shift to produce constructive interference rather than destructive interference between

the fields from the source and its image. This works as the incident wave travels a distance of $\lambda/4$ or 90°, then the PEC ground plane causes the reflected wave to have a 180° phase shift, finally the reflected wave travels a distance of $\lambda/4$ or 90°. Therefore, when the reflected wave returns it will have a phase difference of 360°, causing constructive interference. This effect can be seen in Figure 2.1.1 [5].

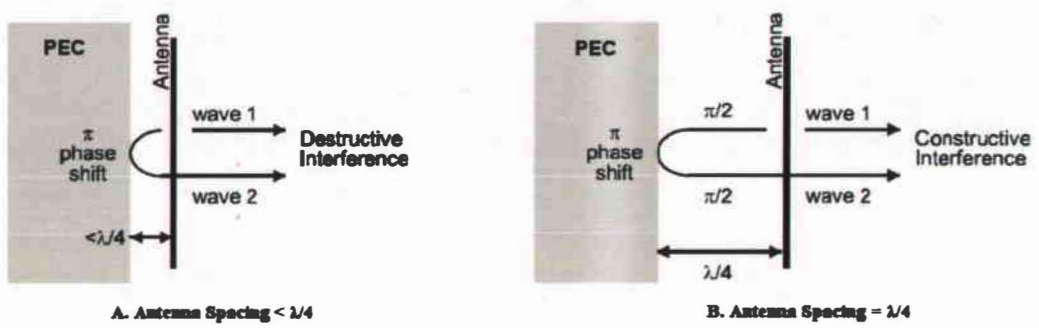

Figure 2.1.1: Effects of PEC Ground Plane Spacing from Antennas

By implementing this spacing, the reverse image currents do not have drastic effects on the antenna's performance. However, as the antenna is moved closer to the PEC ground plane, these image currents interact with the antenna currents and cause the antenna to effectively short circuit. Furthermore, surface-waves can be guided by the PEC and in addition to the associated loss of power, discontinuities may allow these fields to radiate and interfere with the antenna radiation. Examples of this radiation and associated interference can be seen as ripples in the antenna's radiation pattern [5]. The size of the PEC ground plane, as well as the spacing from the antenna can reduce the effects of these surface-waves. These precautions introduce a fixed length between the antenna and the PEC ground plane in terms of λ. Not only does this

fixed spacing limit any further reduction of the antenna's profile, it also limits the bandwidth that the antenna may inherently have.

To overcome the undesirable effects of implementing electrically excited antennas with PECs, research has been done into the implementation of slot antennas, which are equivalently excited by magnetic currents. According to image theory, the implementation of a PEC ground plane with an antenna excited by an equivalent magnetic current will produce an image with currents in the same direction as those in the antenna [3]. Therefore, allowing the antenna to be placed very close to the ground plane without effectively short circuiting the antenna. This magnetic current excitation can be achieved through the use of slot based excitation methods. A highly effective slot array design has been produced by Raytheon (research sponsor) [7]. This design, shown in Figure 2.1.2, produced an effective low-profile, wide-band antenna, however, at the cost of a more elaborate feed structure, particularly, a loop-type feed structure.

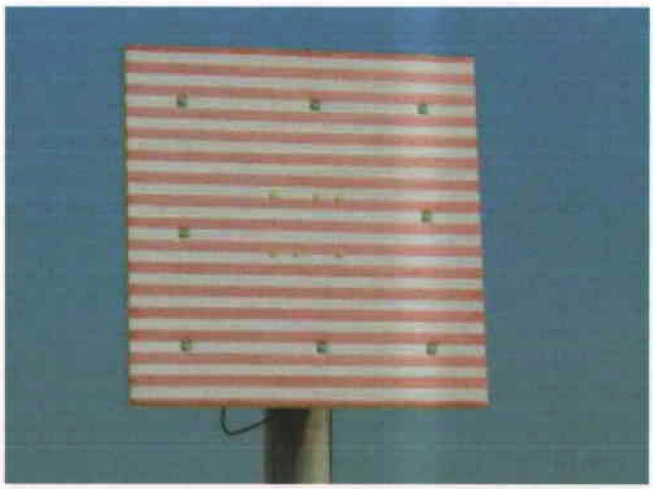

Figure 2.1.2: Raytheon's Wideband Long Slot Array Antenna

An investigation into the development of the slot array design led to the slot spiral antenna design presented in [8] and [9]. Examination of this design shows, to excite the 2nd mode of the slot spiral (producing a null at boresight [8]), the two outer ends of the spiral arms were fed by two individual in phase feed systems. This also resulted in a low-profile antenna, while maintaining a PEC backing. Rather than altering the antenna design, another approach which is based on altering the ground plane design is presented in this thesis to produce an efficient low-profile, wide-band antenna design.

2.2: Alternatives to PEC Ground Planes

It would be optimal to implement an alternative to PEC ground planes with electrically excited antennas. Features of these alternatives include that they do not produce reverse image currents, do not introduce a 180° phase shift for reflected waves, and do not support propagating surface-waves. As previously stated, it would be optimal to back electrically excited antennas with a PMC ground plane. This implementation would provide positive image currents and suppress the propagating surface-waves, while also eliminating the 180° phase shift [3, 5, 6]. A PMC has the properties opposite of those described earlier for a PEC. Rather than a low ratio of electric fields to magnetic fields, a PMC has a high ratio of electric fields to magnetic fields. Therefore, there exists an H-Field node and an E-Field anti-node at the surface. Equation 2.1, through electromagnetic theory, shows the relationship of wave (intrinsic) impedance to the electric and magnetic fields. This equation shows

that a PMC ground plane, with a large ratio of electric fields to magnetic fields, will have a high surface impedance.

$$Z = \frac{E_z}{H_y} \tag{2.1}$$

However, no PMC exists in nature. To produce the desired characteristics of a PMC, it is logical to conclude that the implementation of a high-impedance surface could emulate a PMC. Through research and design, high-impedance surfaces have become a realizable alternative to PMCs. These high-impedance surfaces offer the same desirable qualities that a PMC offers. These qualities make high-impedance surfaces an advantageous ground plane for electrically excited antennas. It is because of the characteristics of high-impedance surfaces that it is possible to maintain the antenna's inherent frequency independence, while also reducing the antenna's profile without adverse effects on the antenna performance. Possible designs of high-impedance surfaces will be described in the following section.

2.3: High-Impedance Surfaces

As discussed earlier, PEC ground planes have very low surface impedances. These low impedances span a wide band of frequencies. However, by altering the texture of the PEC surface, it is possible to increase the surface impedance over a finite bandwidth, producing an electromagnetic band-gap. The period and geometry of the texture used on the surface can be altered to adjust the electromagnetic band-gap for various design specifications [5].

The high-impedance EBG structure designed in this work is the evolution of two types of textured surfaces: bumpy surfaces and corrugated surfaces, shown in Figure 2.3.1 [5]. When the periodicity of these textured surfaces is much smaller than a wavelength of the surface-waves, they can be assigned an impedance that can predict many of their electromagnetic properties [5].

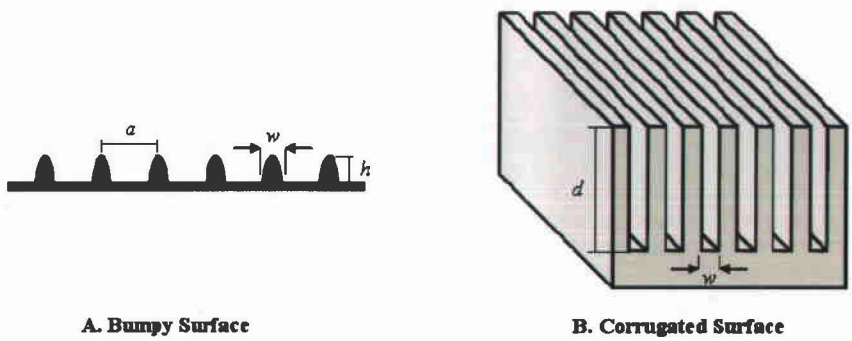

Figure 2.3.1: Bumpy and Corrugated High-Impedance Surfaces

For the case of bumpy surfaces, shown in Figure 2.3.1, when the wavelength of the surface-waves is much larger than the period of bumps (*a*), the waves are unaffected by the bumps. As the wavelength of the surface-waves is decreased, the effect of the bumps becomes more pronounced. The surface-waves reach the Brillouin zone boundary of the structure when the surface-waves have a half-wavelength that fits in the period of bumps. At this boundary the surface-waves have two different modes: the first being where the nulls are centered on the bumps and the second being where the nulls are centered between the bumps. The frequencies that fall between these two modes have surface-waves that aren't allowed to propagate, creating a small electromagnetic band-gap. The size of this electromagnetic band-gap is proportional to the size, height (*h*) and width (*w*), of the

bumps on the textured surface [5]. As the bumps are elongated and the tops stretched towards one another, creating 'thumbtack' like protrusions, the form of the EBG structure used in this work can be seen. Greater capacitances begin to build as the tops of the bumps are stretched closer to one another. Additionally, currents travel a path that circulates between the elongated bumps, creating inductances. The implementation of these 'thumbtacks' allows for a wider electromagnetic band-gap than obtained with the bumps.

The case of the corrugated surface implements a metal slab with a series of vertical slots cut out, as shown in Figure 2.3.1. These slots have widths (w) much smaller than a wavelength and are usually implemented with depths (d) of $\lambda/4$. Each slot can be seen as a parallel plate transmission line that is shorted at the bottom. When the depth of the slot is $\lambda/4$, this short creates the appearance of an open circuit at the surface of the structure. The appearance of this open creates a high impedance at the surface of the structure. The impedance of the slots can be calculated using Equation 2.2 [5], where η is the intrinsic impedance, k is the wave vector, and d is the depth of the slot.

$$Z = j\eta \tan(kd) \tag{2.2}$$

The intrinsic impedance (η) and the wave vector (k) are described in Equations 2.3 and 2.4 [5] respectively.

$$\eta = \sqrt{\frac{\mu}{\varepsilon}}$$

(2.3)

$$k = \frac{\omega}{c}\sqrt{\frac{\varepsilon}{1+\varepsilon}}$$

(2.4)

Because the structure is designed with the slots much thinner than a wavelength, the surface can be assigned an impedance equal to that of the slots [5]. As these slots are altered and folded to once again create 'thumbtack' like protrusions, the EBG structure in this work can be seen. The folding of the slots allows for a reduction in profile of the structure and an increased band-gap.

Since the high-impedance EBG structure designed in this work is an evolution of both bumpy surfaces and corrugated surfaces, it has properties similar to these surfaces. These attractive properties include: over an electromagnetic band-gap, there are positive image currents, waves are reflected with little or no phase shift, and surface-wave propagation is suppressed. Figure 2.3.2 [5] shows that as an antenna is spaced much less than a distance of λ from the EBG structure there is no phase shift and, therefore, no destructive interference, allowing the antenna to operate with no loss in performance. Additionally, the designed EBG structure offers a wider band-gap than using a bumpy surface and a lower profile than using a corrugated surface [5]. The properties offered by the designed EBG structure are desirable characteristics for the backing of electrically excited antennas.

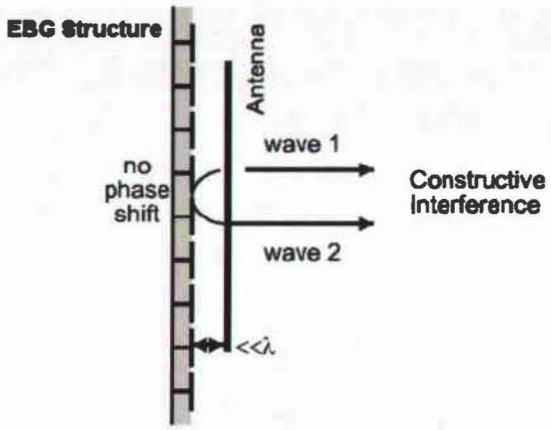

Figure 2.3.2: Effects of EBG Structure Spacing from Antennas

2.4: Design of EBG Structures

Two methods have been developed for the design of the EBG structures presented in this thesis. The first of these methods is based on a parallel LC circuit model of the EBG structure and the second is based on the wavelength of the desired resonant frequency. The accuracy of these methods is shown, in this work, through the design and analysis of the EBG structure implemented with dipole antennas and Archimedean spiral antennas. The correlation between both methods in the design of the EBG structure and the results produced by the designed structure verify the effectiveness of both methods to design an optimal EBG structure. Using either of these methods or a combination of both provides an accurate starting point for designing an EBG structure to implement as a ground plane for antennas. However, as with any design method, these methods will not always provide perfect results. The methods offered provide an accurate starting point from which to optimize the

various design parameters. The results presented in this thesis show that an optimally designed EBG structure will work for implementation with various types of antenna designs, i.e., dipole antennas and spiral antennas.

As mentioned earlier, the geometry of the EBG structure designed in this work was developed from altering the geometries of the bumpy and corrugated surfaces described previously. The EBG structure that evolved from these high-impedance surfaces is shown in Figure 2.4.1.

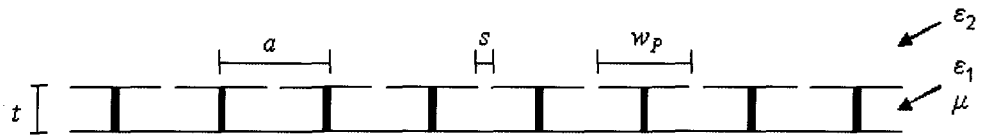

Figure 2.4.1: High-Impedance Electromagnetic Band-Gap Structure

To design the geometry of the EBG structure, the parallel LC circuit model and wavelength-based model design methods are presented next.

In the case of the parallel LC circuit model, the EBG structure is characterized by an equivalent LC circuit, shown in Figure 2.4.2 [5].

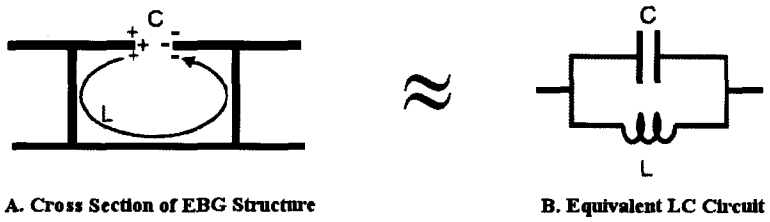

Figure 2.4.2: EBG Structure and Equivalent Parallel LC Circuit

The capacitances induced are a combination of the capacitances between the patches and the sheet capacitance in the EBG structure. The combination of these capacitances is characterized in Equation 2.5 [5], where the first term comes from the

capacitances between the patches and the second comes from the sheet capacitance in the EBG structure.

$$C = \frac{w_P(\varepsilon_1 + \varepsilon_2)}{\pi}\cosh^{-1}\left(\frac{a}{s}\right) + \varepsilon_1 t$$

(2.5)

In this equation w_P is the width of the patches shown in Figure 2.4.1, ε_1 and ε_2 are the electric permittivity inside the EBG structure and surrounding the EBG structure respectively, a is the period of the 'thumbtack' protrusions shown in Figure 2.4.1, s is the spacing between the patches shown in Figure 2.4.1, and t is the thickness of the EBG structure shown in Figure 2.4.1. The inductances are induced by currents circulating between the 'thumbtack' protrusions of the EBG structure. The induced inductances are characterized by Equation 2.6 [5].

$$L = \mu t$$

(2.6)

In this equation μ is the magnetic permeability inside the EBG structure and t is the thickness of the EBG structure shown in Figure 2.4.1. By describing the structure with a simple LC circuit, the impedance of the structure can be calculated using basic circuit theory. Equation 2.7 describes how the impedance is calculated for a parallel LC circuit.

$$Z = \frac{j\omega L}{1 - \omega^2 LC}$$

(2.7)

As circuit theory describes, an LC circuit has a certain resonant frequency that can be calculated using Equation 2.8.

$$\omega_0 = \frac{1}{\sqrt{LC}} \tag{2.8}$$

Figure 2.4.3 shows the impedance of the EBG structure, as calculated with the parallel LC circuit model, and its relationship to frequency.

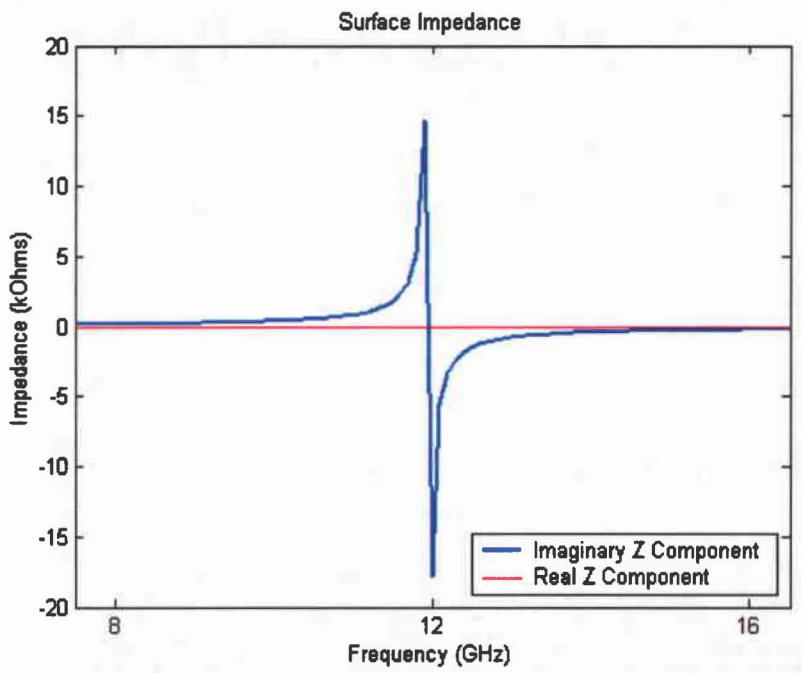

Figure 2.4.3: Impedance of a Parallel LC Circuit

As the figure depicts, at the resonant frequency the impedance is very high. Circuit theory explains that a positive imaginary impedance component is associated with inductance and a negative imaginary impedance component is associated with capacitance. Therefore, at frequencies below the resonant frequency, the structure

will act inductively and at frequencies above the resonant frequency, the structure will act capacitively. Additionally, as shown in the figure, the impedance is purely imaginary. Therefore, the only losses introduced by the structure are associated with dielectric and conduction losses [5]. Around the resonant frequency, there is an electromagnetic band-gap where the impedance is very high. This band-gap, or the bandwidth of the structure, can be calculated using Equations 2.9-2.12 [5].

$$\omega = \omega_0 \sqrt{1 \pm \frac{Z_0}{\eta}} \tag{2.9}$$

Where Z_0 can be viewed as the characteristic impedance of the surface and is described in Equation 2.10.

$$Z_0 = \sqrt{\frac{L}{C}} \tag{2.10}$$

Because Z_0 is much smaller than η, Equation 2.9 can be reduced to Equation 2.11.

$$\omega \approx \omega_0 \left(1 \pm \frac{Z_0}{2\eta} \right) \tag{2.11}$$

$$B.W. = \frac{\Delta\omega}{\omega_0} = \frac{Z_0}{\eta} \tag{2.12}$$

The structure loses its high-impedance properties outside of this band-gap. As shown earlier, the structure behaves inductive at frequencies below the band-gap and capacitive at frequencies above the band-gap. The inductive behavior at frequencies

below the band-gap will support TM surface-waves, while the capacitive behavior at frequencies above the band-gap will support TE surface-waves [5].

For the wavelength-based design method, the geometries are designed using equations based on the wavelength of the desired resonant frequency. This method was developed by observing, through research and design, the relationship of the EBG structure geometry to the resonant frequency of the structure. Through these observations, relationships between the various EBG structure geometries and the wavelength of the resonant frequency are described with equations. These equations provide a direct correlation between the structure's geometries and the wavelength of the desired resonant frequency. The geometries of the EBG structure can be seen in Figure 2.4.4.

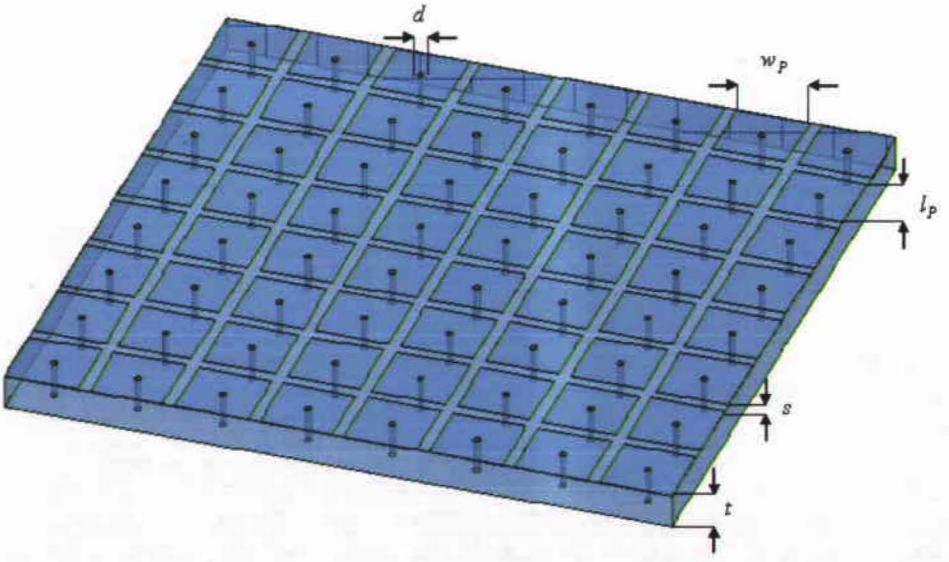

Figure 2.4.4: High-Impedance Electromagnetic Band-Gap Structure

The equations developed, from the observed relationships, to design the various geometries of the EBG structure can be seen in Equation 2.13 [6, 10].

$$
\begin{aligned}
l_P &= w_P = 0.12\lambda \\
s &= 0.02\lambda \\
d &= 0.01\lambda \\
t &= 0.057\lambda
\end{aligned}
\tag{2.13}
$$

In these equations l_P and w_P are the length and the width of the patches shown in Figure 2.4.4 respectively, s is the spacing between the patches shown in Figure 2.4.4, d is the diameter of the vias shown in Figure 2.4.4, and t is the thickness of the EBG structure shown in Figure 2.4.4.

Specifically, the EBG structure presented in this thesis is initially designed with the wavelength-based model. This structure is designed with an operating frequency of 12GHz (λ = 25mm). Using this wavelength in Equation 2.13, an EBG structure, shown in Figure 2.4.4, is designed with the following geometries: $l_P = w_P =$ 3mm, s = 0.5mm, d = 0.25mm, and t = 1.425mm. Additionally, to show the accuracy and effectiveness of both the parallel LC circuit model and the wavelength-based model, the geometries of the wavelength-based model designed EBG structure are plugged into the parallel LC circuit model. From these geometries, the induced capacitances are calculated to be 0.099pF and the induced inductances are calculated to be 1.79nH. These induced capacitances and inductances result in a resonant frequency of 11.9GHz. The correlation between the two design methods provides initial verification for the accuracy of both methods. Ultimately, verification of both design methods is done through simulations using Ansoft HFSS. These design methods are validated through the examination of results produced by the simulations

and the observation of the characteristics of a $\lambda/2$ dipole antenna and an Archimedean spiral antenna placed above the designed EBG structure. These results and observations will be discussed in the following chapters.

CHAPTER 3: DESIGN AND IMPLEMENTATION OF EBG STRUCTURES WITH DIPOLE ANTENNAS

To reduce the profile of a dipole antenna structure and to obtain a unidirectional beam, it is necessary to back the antenna with an optimal structure. Dipole antennas, because they are electrically excited, do not function effectively when placed at a small distance over a PEC ground plane. This is due to, as previously mentioned, the properties of PEC ground planes. PEC ground planes, when used to back electrically excited antennas, produce reverse image currents, introduce a phase offset of 180° for reflected waves, and support propagating surface-waves [3, 4, 5]. According to electromagnetic theory, it would be optimal to place a dipole over a PMC ground plane. PMC ground planes, when implemented with electrically excited antennas, produce positive image currents, do not introduce a phase offset for reflected waves, and suppress propagating surface-waves [3, 5, 6]. However, as stated earlier, no PMC exists in nature. To produce the desired properties of a PMC, high-impedance EBG structures have been implemented as a realizable alternative.

3.1: EBG Structure Design and Dipole Antenna Implementation

The EBG structure design presented in this thesis is developed from designs available in published literature. The two references used primarily when designing the EBG structure presented in this work are [6] and [10]. The structures presented in these references were designed for 12GHz and had the following parameters in common: $l_P = w_P = 0.12\lambda$ (3mm), $t = 0.04\lambda$ (1.0mm), $h = 0.02\lambda$ (0.5mm), $\varepsilon_{r1} = 2.2$,

and $\varepsilon_{r2} = 1$, where l_P and w_P are the patch length and width respectively, t is the EBG structure thickness, h is the spacing between the antenna and the structure, and ε_{r1} and ε_{r2} are the relative permittivity inside and outside the EBG structure respectively. While [10] does not specify the patch spacing (s) or the via diameter (d), [6] defines them as: $s = 0.02\lambda$ (0.5mm) and $d = 0.01\lambda$ (0.25mm).

Using a wavelength-based model similar to that seen in [6] and [10] and the parallel LC circuit model, an EBG structure is designed, using Ansoft HFSS, to back a $\lambda/2$ dipole for operation at 12GHz. The EBG structure, shown in Figure 3.1.1, designed in terms of λ for future scalability, is designed with the following parameters: $l = w = 1.1\lambda$ (27.5mm), $l_P = w_P = 0.12\lambda$ (3mm), $s = 0.02\lambda$ (0.5mm), $d = 0.01\lambda$ (0.25mm), $t = 0.057\lambda$ (1.425mm), $h = 0.02\lambda$ (0.5mm), $\varepsilon_{r1} = 2.2$, and $\varepsilon_{r2} = 1$.

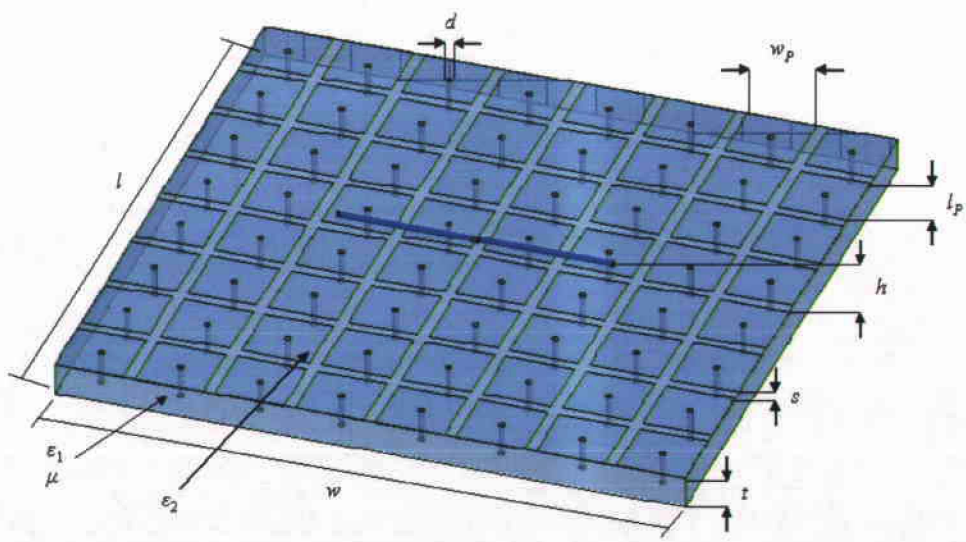

Figure 3.1.1: EBG Structure with $\lambda/2$ Dipole Antenna

The dipole antenna implemented with the EBG structure is designed with a length of 0.48λ (12mm) and a diameter of 0.01λ (0.25mm).

3.2: EBG Structure and Dipole Antenna Analysis and Results

Initially, the dipole antenna is simulated in free space to validate the accuracy of the simulation software used, Ansoft HFSS. Ansoft HFSS produced a directivity, shown in Figure 3.2.1, of 2.55dB (1.8), which correlates well with the published value of 2.15dB (1.64) [11]. This correlation sufficiently validates the accuracy of Ansoft HFSS.

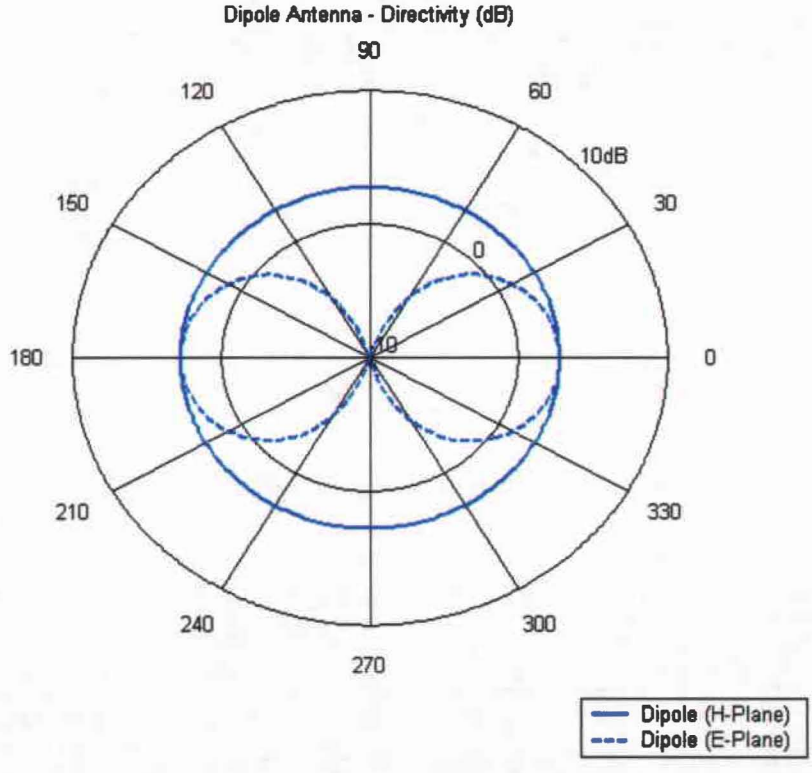

Figure 3.2.1: Directivity of $\lambda/2$ Dipole Antenna

Once the software accuracy was validated, the EBG structure design implemented with the dipole antenna is analyzed. To validate the design, the directivity of the dipole antenna at 0.02λ above the EBG structure and the directivity of the dipole at 0.02λ above a PMC ground plane are compared. The comparison,

shown in Figure 3.2.2, shows good correlation between the directivity values of the dipole above the designed EBG structure and above a PMC ground plane. The correlation of results clearly depicts the validity of the EBG structure design to emulate a PMC ground plane. Additionally, backing the dipole with the EBG structure produces a directivity of 8dB, which correlates well with the results published in [6].

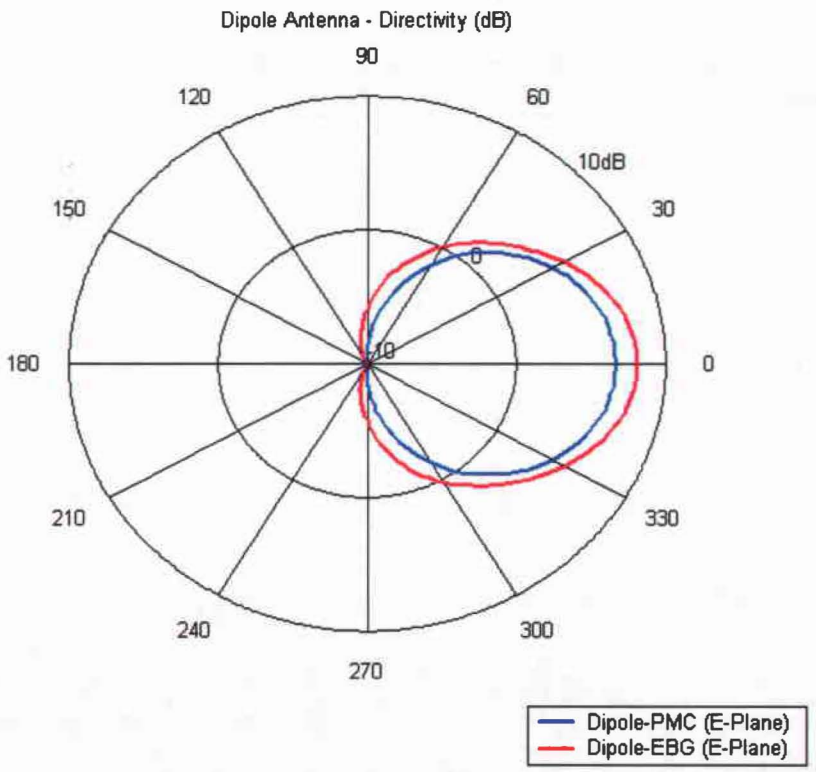

Figure 3.2.2: Directivity of $\lambda/2$ Dipole above PMC and EBG Structure

To show the adverse effects of moving a PEC ground plane too close to the dipole, the return losses (S_{11}) of the dipole in free space, the dipole at 0.02λ above the EBG structure, and the dipole at 0.02λ above a PEC ground plane are compared. This comparison, shown in Figure 3.2.3, shows that placing the dipole antenna too close to

a PEC ground plane effectively short circuits the antenna. Not only does the comparison show the adverse effects of bringing the dipole too close to a PEC ground plane, it also shows that backing the dipole antenna with the designed EBG structure improves the return loss significantly, thus, improving antenna performance.

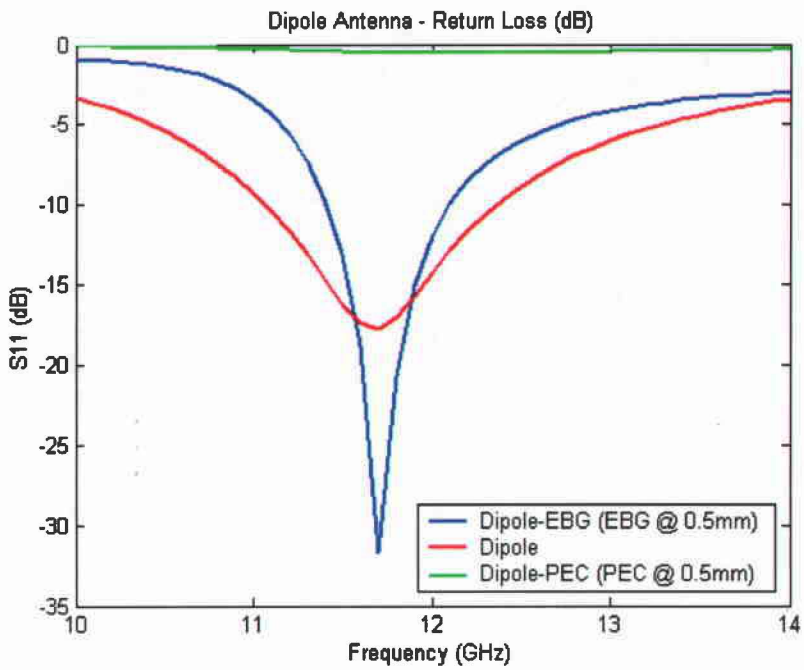

Figure 3.2.3: S_{11} of $\lambda/2$ Dipole in free space, above PEC, and EBG Structure

CHAPTER 4: DESIGN AND IMPLEMENTATION OF EBG STRUCTURES WITH SPIRAL ANTENNAS

As shown previously, antennas excited with electric current do not perform efficiently over a PEC at close distances. By using an EBG structure to emulate a PMC ground plane, positive image currents, little or no phase shift for reflected waves, and surface-wave suppression are obtained at close distances to antennas excited with electric current. According to the parallel LC circuit model, an EBG structure will have a certain bandwidth in which it maintains its PMC properties. To fully explore the possibilities of the effectiveness of implementing an EBG structure as a ground plane, it is optimal to test the implementation with an inherently wide-band antenna. Since Archimedean spiral antennas are traditionally excited with electric current and are inherently wide-band, it is clear that they are a good candidate for implementation with an EBG structure. This implementation will allow for a reduced antenna profile without harmful effects on the antenna's performance.

4.1: Archimedean Spiral Antennas

There are various reasons why an Archimedean spiral antenna is chosen for implementation, a couple of these being: their ease to manufacture using printed circuit techniques and because the Archimedean spiral is linearly proportional to the polar angle, it flares much slower than an equiangular spiral, which is exponentially proportional to the polar angle, thus, keeping the antenna more compact [1]. An Archimedean spiral, shown in Figure 4.1.1, is constructed with two arms that are wound at a constant spacing from one another.

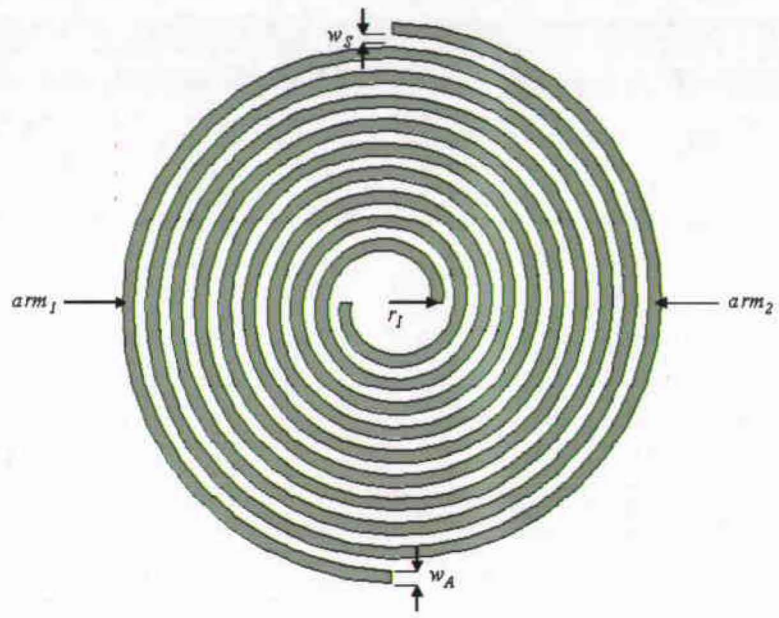

Figure 4.1.1: Archimedean Spiral Antenna

As stated earlier, the spiral arms are linearly proportional to the polar angle (ϕ) and their radii are described in Equation 4.1, where r_0 is the proportionality constant described in Equation 4.2 and r_I is the inner radius of the spiral [12]. In Equation 4.2, w_S is the arm spacing width and w_A is the arm width.

$$r_{arm_1} = r_0\phi + r_I$$
$$r_{arm_2} = r_0(\phi - \pi) + r_I \tag{4.1}$$

$$r_0 = \frac{w_S + w_A}{\pi} \tag{4.2}$$

If the spacing between the arms is equal to the thickness of the arms, the spiral antenna becomes self-complimentary. The input impedance of a complimentary

antenna is found using Babinet's principle, this impedance can be calculated using Equation 4.3.

$$Z_{metal} Z_{air} = \frac{\eta^2}{4} \tag{4.3}$$

For a self-complimentary antenna this reduces to: $Z_{metal} = Z_{air} = \eta/2 = 188.5\Omega$. To counteract the 180° phase offset introduced by the half-turn distance, or $\lambda/2$ path differential, between the two arms, the spiral arms are fed at a phase offset of 180°. This excites the 1st mode of the spiral (producing maximum gain at boresight [8]) and produces constructive interference in the region where the antenna arms are radiating, or the active region. The active region occurs at a point where the circumference of the spiral is equal to the wavelength of the active frequency. This point can be calculated in terms of the spiral's radius using geometry, $c = 2\pi r$. Therefore, since the active region occurs at $c = \lambda$, then $2\pi r = \lambda$. Solving for r in this equation gives the active region in terms of the radius.

$$r_A = \frac{\lambda}{2\pi} \tag{4.4}$$

This active region will occur at two points that are diametrically opposite from one another with respect to the center of the spiral. These points will radiate with equal intensity but with a relative phase difference of 90°, therefore, creating radiated fields that are circularly polarized. Prior to the active region the electrical distance to adjacent points on the spiral arms is electrically small. This, in turn, keeps the phase

offset introduced by the excitation, causing the arms to be in transmission line mode with little radiation. Beyond the active region the currents in the antenna arms are very weak, due to losses from radiation, causing the antenna to effectively behave infinite in length. As the frequency is altered, the active region either moves inwards, for higher frequencies, or outwards, for lower frequencies, on the spiral arms with unchanging antenna performance. This allows the antenna to be self-scaling for a band of frequencies, thus, creating a wide-band antenna [1].

4.2: Archimedean Spiral Antenna Design

To implement the EBG structure previously designed for the dipole antenna, an Archimedean spiral, shown in Figure 4.2.1, is designed with a center frequency of 12GHz and a frequency range of 8-16GHz.

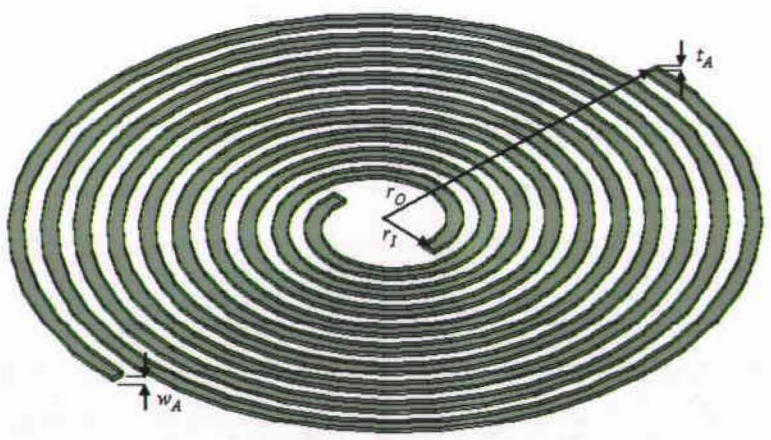

Figure 4.2.1: Archimedean Spiral Antenna

The width and height of the spiral antenna arms are designed at: $w_A = 0.016\lambda$ (0.4mm) and $t_A = 0.004\lambda$ (0.1mm) respectively. The spiral arms are spaced at a distance of 0.016λ (0.4mm) to produce a self-complimentary structure. The inner and

outer radii of the spiral arms are designed using equations similar to Equation 4.4. To ensure that the active regions for the highest and lowest frequencies of the desired bandwidth are located on the antenna, the inner radius is decreased by 50% while the outer radius is increased by 50%. Using this ideology, the inner and outer radii were designed to be: $r_I = 0.5*(\lambda_H/2\pi)$ and $r_O = 1.5*(\lambda_L/2\pi)$ respectively, with r_I being 1.5mm and r_O being 9mm.

4.3: EBG Structure and Archimedean Spiral Antenna Implementation

After the Archimedean spiral antenna design was completed, it is implemented with the EBG structure previously designed for the dipole antenna. The designed EBG structure, shown in Figure 4.3.1, has the following parameters: $l = w = 1.1\lambda$ (27.5mm), $l_P = w_P = 0.12\lambda$ (3mm), $s = 0.02\lambda$ (0.5mm), $d = 0.01\lambda$ (0.25mm), $t = 0.057\lambda$ (1.425mm), $h = 0.02\lambda$ (0.5mm), $\varepsilon_{r1} = 2.2$, and $\varepsilon_{r2} = 1$.

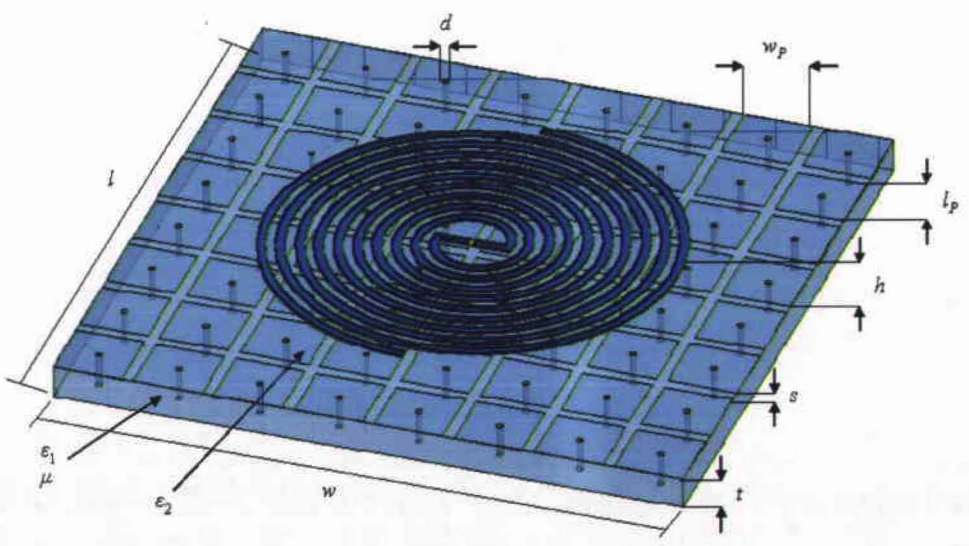

Figure 4.3.1: EBG Structure with Archimedean Spiral Antenna

4.4: EBG Structure and Archimedean Spiral Antenna Analysis and Results

To validate the effectiveness of backing the Archimedean spiral antenna with the EBG structure, a comparison is made between the gain values of the Archimedean spiral antenna at the traditional design distance of $\lambda/4$ above a PEC ground plane, at a distance of 0.02λ or $\lambda/50$ above a PMC ground plane, and at $\lambda/50$ above the EBG structure. The comparison, shown in Figure 4.4.1, shows good correlation between the gain values of the Archimedean spiral above the EBG structure and above a PMC ground plane.

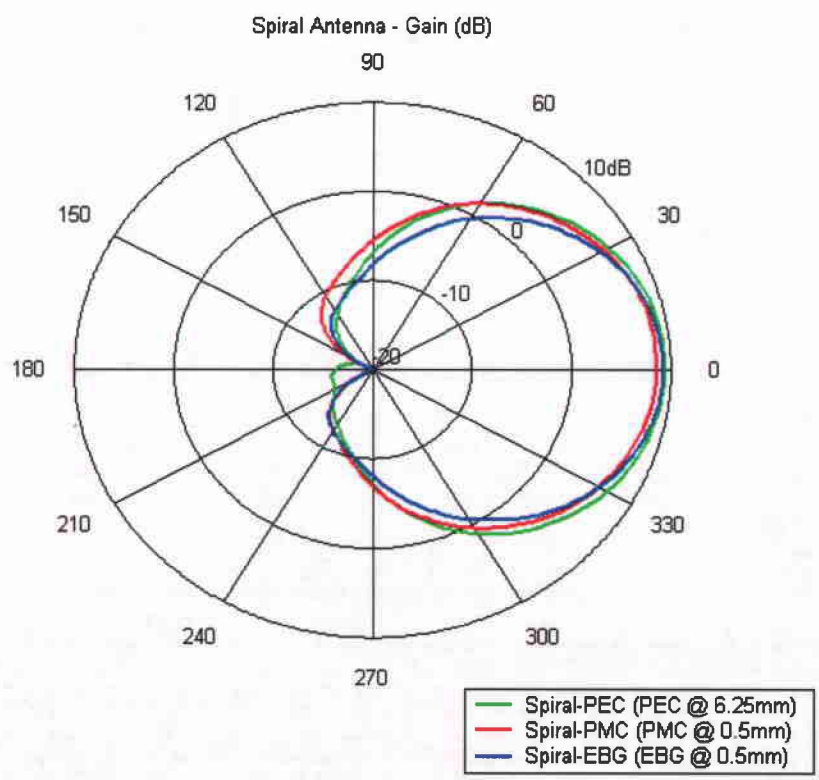

Figure 4.4.1: Gain of Spiral Antenna above PEC, PMC, and EBG Structure

The correlation of results shows, once again, the effectiveness of the EBG structure to emulate a PMC ground plane. The comparison also shows that placing the spiral

antenna over the EBG structure, rather than a PEC ground plane, produces an antenna height reduction of 92% without compromising performance. Additionally, the results show that all three implementations have a gain of approximately 9dB.

To show the adverse effects of placing a PEC ground plane too close to the spiral antenna, the return losses (S_{11}) of the Archimedean spiral in free space, at $\lambda/4$ above a PEC ground plane, at $\lambda/50$ above a PEC ground plane, at $\lambda/50$ above the EBG structure, and at $\lambda/50$ above a PMC ground plane are compared. This comparison, shown in Figure 4.4.2, shows that placing a PEC ground plane too close to the spiral antenna effectively short circuits the antenna.

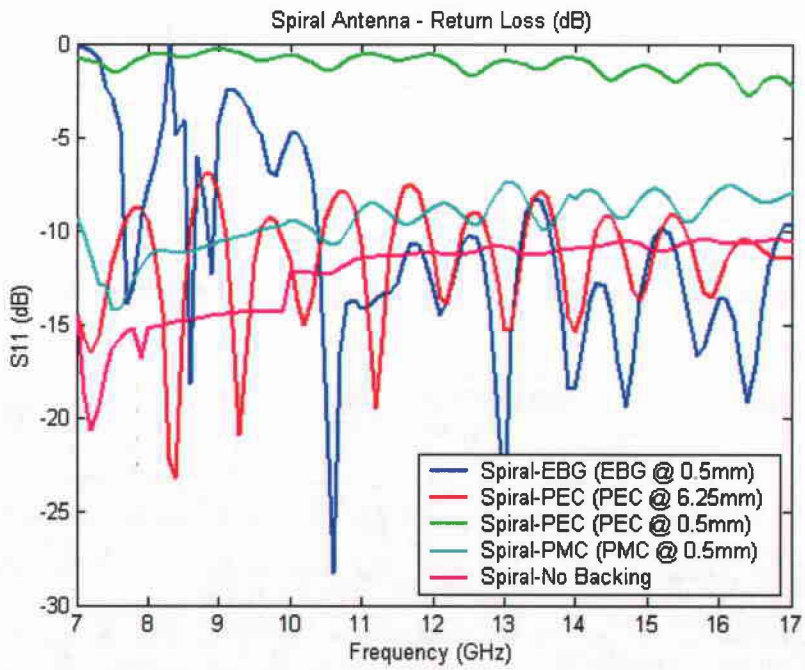

Figure 4.4.2: S_{11} of Spiral Antenna in free space, above PEC, PMC, and EBG Structure

Additionally, the comparison shows that placing the spiral at $\lambda/50$ above the EBG structure provides improvement in return loss over placing the spiral at $\lambda/4$ above a

PEC ground plane as well as at $\lambda/50$ above a PMC ground plane. The return loss for the Archimedean spiral above the EBG structure shows that the novel implementation maintains 71% (10.3-16GHz) of the Archimedean spiral's designed bandwidth (8-16GHz). Backing spiral antennas with properly designed EBG structures, therefore, provides a low-profile antenna and also maintains a considerable fraction of the spiral antenna's inherent broadband behavior.

An analysis of the induced fields on the surface and inside of the EBG structure is done to obtain a better understanding of the complex interactions between the spiral antenna and the designed EBG structure. The results of this analysis can be seen in Figure 4.4.3.

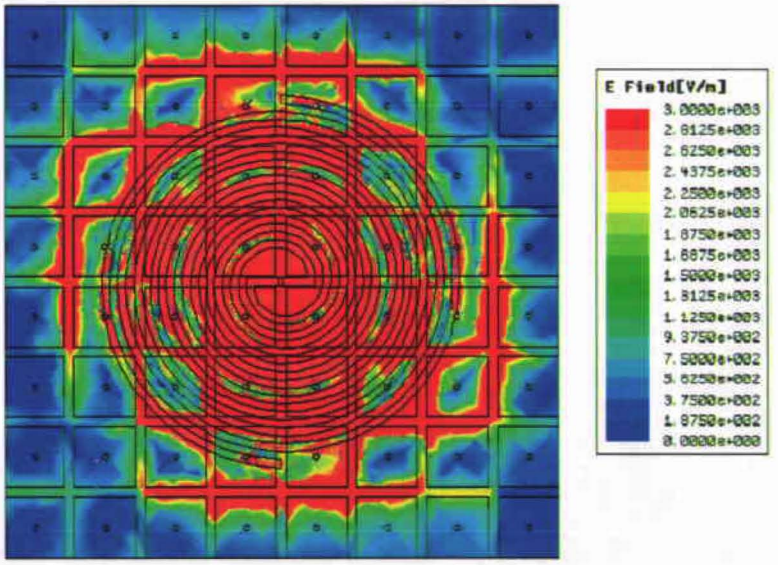

A. Capacitances induced between patches

B. Inductances induced between 'thumbtack' protrusions

Figure 4.4.3: Field Interactions with EBG Structure

As previously discussed, the EBG structure obtains its desirable characteristics from the high impedance created by the induced capacitances and inductances of the structure. The results of the analysis clearly depict the fields between the patches that induce the capacitances as well as the fields circulating between the 'thumbtack' protrusions that induce the inductances. Therefore, this analysis further validates the previous notions of field interactions with the high-impedance EBG structure.

CHAPTER 5: SCALED IMPLEMENTATION OF ANTENNAS AND EBG STRUCTURES

The EBG structure presented in this thesis was initially designed for operation around 12GHz to coincide with previously published literature. As with any antenna structure, scalability is an important factor to consider when examining the features of new designs. The ease of scalability is a great contribution to the efficiency of the design process and, therefore, greatly affects the appeal of the design. Other recent work done by Raytheon (research sponsor) in the area of low-profile, wide-band antennas has focused on a bandwidth centered around 1.2GHz. This previous work prompted a test of the scalability for the EBG structure at the frequency of 1.2GHz. Because the structure is designed in terms of λ, it is a relatively simple process to scale the geometries and simulate the overall scaled design. The parameters of the scaled EBG structure are: $l = w = 1.1\lambda$ (27.5cm), $l_P = w_P = 0.12\lambda$ (3cm), $s = 0.02\lambda$ (0.5cm), $d = 0.01\lambda$ (0.25cm), $t = 0.057\lambda$ (1.425cm), $h = 0.02\lambda$ (0.5cm), $\varepsilon_{r1} = 2.2$, and $\varepsilon_{r2} = 1$.

5.1: Scalability of the EBG Structure with Dipole Antennas

To test the scalability of the EBG structure we initially used the simple case of a $\lambda/2$ dipole at 1.2GHz. The dipole antenna is designed with a length of 0.48λ (12cm) and a diameter of 0.01λ (0.25cm). This scaled implementation can be seen in Figure 5.1.1. A comparative analysis of the simulated results for the original design and the scaled design is done to verify the effectiveness of the designed structure's scalability. The results from this analysis, as Figure 5.1.2 depicts, shows that the

directivity values for the EBG structure and dipole design at 12GHz and the scaled design at 1.2GHz match up perfectly.

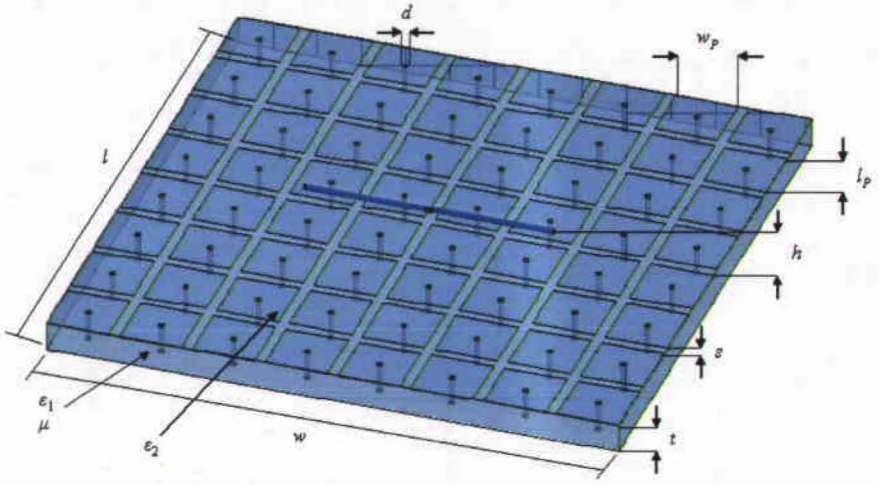

Figure 5.1.1: Scaled EBG Structure with Dipole Antenna

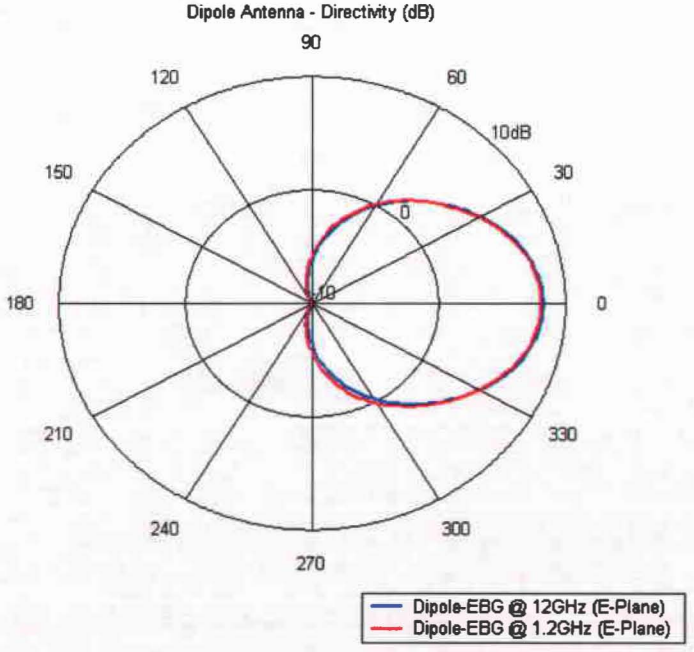

Figure 5.1.2: Directivity of $\lambda/2$ Dipole above EBG Structure at 12GHz and 1.2GHz

The correlation of results, therefore, verifies that the EBG structure and dipole antenna design is fully scalable.

5.2: Scalability of the EBG Structure with Spiral Antennas

After the scalability of the EBG structure and dipole antenna implementation was tested and validated, the scalability of the EBG structure and Archimedean spiral antenna design is tested. As with the case of the EBG structure and dipole, the implemented design of the EBG structure and spiral antenna is scaled to 1.2GHz. The geometries of the scaled spiral antenna design are: $w_A = 0.016\lambda$ (0.4cm), $t_A = 0.004\lambda$ (0.1cm), $r_I = 0.5*(\lambda_H/2\pi)$ (1.5cm), and $r_O = 1.5*(\lambda_L/2\pi)$ (9cm). The geometry of the scaled spiral antenna can be seen in Figure 5.2.1.

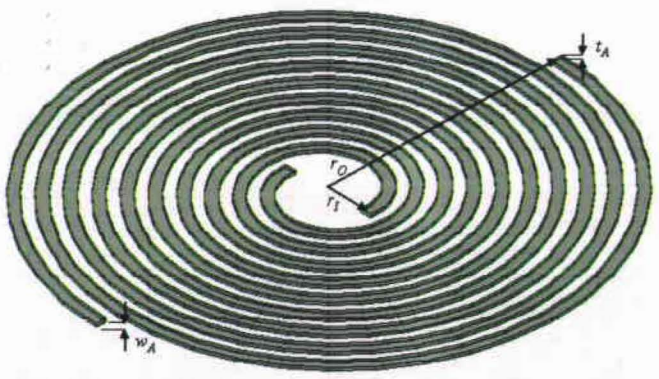

Figure 5.2.1: Scaled Archimedean Spiral Antenna

The scaled EBG structure and spiral antenna design can be seen in Figure 5.2.2. As with the scaled EBG structure and dipole implementation, a comparative analysis is performed on the simulation results of the original EBG structure and spiral antenna design and the scaled EBG structure and spiral antenna design. The results of this analysis can be seen in Figure 5.2.3. As depicted by the results of the analysis, the

gain of the EBG structure and spiral design at 12GHz matched up perfectly to the gain of the scaled design at 1.2GHz.

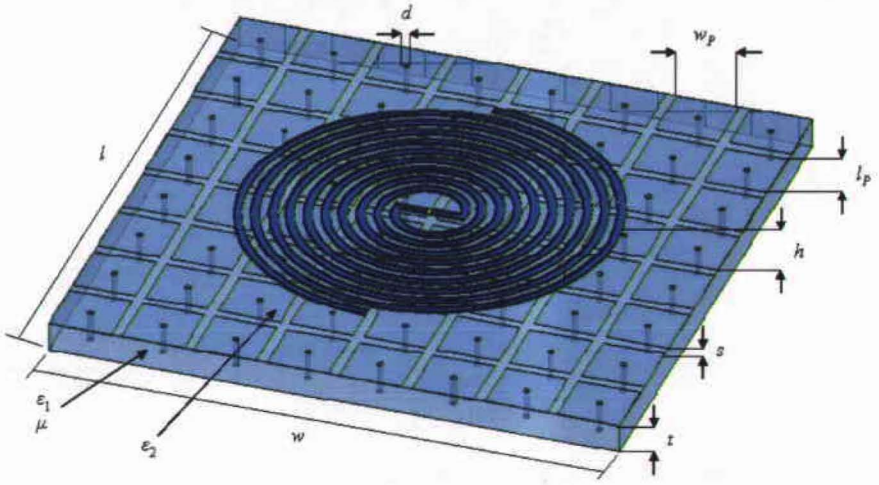

Figure 5.2.2: Scaled EBG Structure with Spiral Antenna

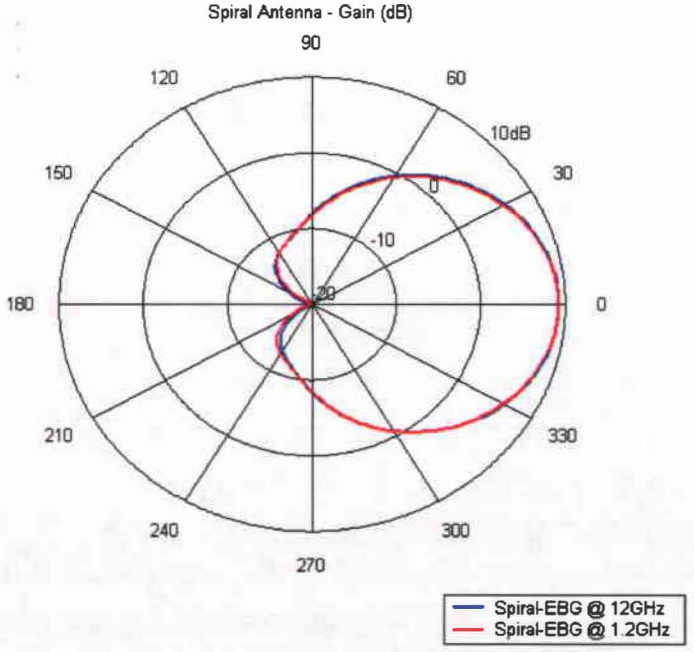

Figure 5.2.3: Gain of Spiral Antenna above EBG Structure at 12GHz and 1.2GHz

The simplicity of the scaling process and the results of the comparative analysis prove the efficiency and effectiveness of the scalability for the EBG structure and Archimedean spiral antenna design.

CHAPTER 6: CONCLUSION

With the phenomenal advances in the area of wireless communications, there is a continued need for devices that cover the specifications of a broader range of applications while maintaining their compact and low-cost features. The increasing complexity of wireless and mobile devices requires an increasing number of components per device and this requires efficient management of available and often very limited space. One avenue for effectively managing the device size is to compact the size of the device's antennas and to use fewer antennas for a broader range of applications. To cover the wide range of applications offered by modern and evolving wireless devices, antennas must efficiently operate at a wide band of frequencies. Thus, a demand for a high-performance, low-cost, low-profile, wide-band antenna arises and has recently become a necessity.

Spiral antennas boast the characteristics vital for implementation in many of these devices and their related diverse applications. They are inherently wide-band antennas, of relatively low profile, and are simple and of low cost to manufacture. Spiral antennas, with these and other characteristics, are enticing candidates for a wide variety of wireless applications, including sensors on airborne, shipboard, and space systems, mobile wireless devices, and for military navigation, sensing, and detection applications.

Traditional implementation of spiral antennas, however, is usually associated with backing the antenna by a PEC ground plane. This results in an often desirable unidirectional radiation pattern, but also results in limiting the antenna performance in

a variety of ways. These include impact on the radiation efficiency and the input impedance value. Due to reverse image currents, the distance between the antenna and ground plane needs to be $\lambda/4$ to provide constructive interference between source and image fields, and at such heights there will be unsuppressed propagating surface-waves. Therefore, it is highly desirable that an alternative procedure for backing spiral antennas that produces a unidirectional radiation pattern be developed. In this thesis, a novel implementation for an Archimedean spiral antenna and EBG structure is presented. The developed design eliminates the undesirable characteristics introduced by the PEC ground plane and provides a ground plane that effectively emulates the much desired features of a PMC. The novel implementation, therefore, provides a high-performance design that is also low-cost and low-profile, while maintaining a considerable fraction of the spiral antenna's broadband characteristics.

6.1: Summary of Efforts and Results

As mentioned earlier, PMCs offer an enticing option for implementation as a ground plane backing for electrically excited antennas. PMCs offer a high-impedance surface due to their high ratio of electric fields to magnetic fields. This high impedance eliminates the drawbacks associated with PEC ground planes. However, no PMC exists in nature. Therefore, research and design has been done to develop surfaces that can emulate a PMC. Through these research and design efforts, high-impedance surfaces, specifically electromagnetic band-gap (EBG) structures, have been developed as a realizable alternative to PMCs.

Two effective EBG structure design methods were presented in this work. The first utilizes a parallel LC circuit model method and the second implements a procedure based on the resonant frequency wavelength. The high impedance of the EBG structure is produced by capacitances and inductances induced by the geometry of the structure. Therefore, the structure was modeled using a simple parallel LC circuit model. This model can be used, through basic circuit and electromagnetic relationships, to design an EBG structure for implementation with wide-band antennas. Additionally, through observing the relationship between the EBG structure geometries and the resonant frequency, a modified wavelength-based model was presented. The correlation shown between these two methods and the results produced by structures designed using these methods validate the accuracy of both to design an effective EBG structure.

The analyses presented in this thesis were started by developing an EBG structure that effectively operates at 12GHz. This design was then tested through implementation with two types of antennas. The effectiveness of the EBG structure to emulate a PMC was first verified for the simple case of a $\lambda/2$ dipole. The directivity of the dipole antenna above the EBG structure and the directivity of the dipole antenna above a PMC ground plane were simulated and the results were compared. The correlation of these results verified the effectiveness of the EBG structure to emulate a PMC. Additionally, the return losses for the dipole when placed in free space, above a PEC ground plane, and above the EBG structure were simulated and the results were analyzed and compared. This analysis showed the

undesirable effects of bringing a PEC too close to the antenna and showed the improvements in antenna performance of implementing the dipole with the designed EBG structure. After verifying the effectiveness of the EBG structure using a dipole antenna, the designed EBG structure was implemented with an Archimedean spiral antenna. A comparison study was then conducted to simulate and analyze the characteristics of the spiral when placed in free space, above a PEC, above a PMC, and above the EBG structure. This comparison study proved the validity of the EBG structure to emulate a PMC ground plane over a considerable fraction of the spiral's inherent bandwidth. Additionally, through this comparison, the undesirable effects of bringing a PEC ground plane too close to the spiral were clearly demonstrated. The comparison also showed antenna performance improvement for the case of the EBG structure over the traditional PEC ground plane implementation through the positive image and, hence, the enhanced radiation in the desired unidirectional pattern. Finally, the designed EBG structure and Archimedean spiral antenna's scalability was tested and validated.

This work presented the novel implementation of an EBG structure and an Archimedean spiral antenna. This design offers a 92% height reduction over traditional Archimedean spiral design without adverse effects on the spiral's performance. The presented results show that this design offers a gain of 9dB with 71% of the Archimedean spiral's designed bandwidth. The design presented in this thesis, therefore, offers a high-performance, low-cost, low-profile, wide-band antenna.

6.2: Future Work

This thesis has shown that by implementing an EBG structure with an inherently wide-band Archimedean spiral antenna, it is possible to maintain some of the antenna's inherent broad bandwidth. However, the Archimedean spiral designed in this work offers more bandwidth than what has been currently sustained by the EBG structure. Future work on the EBG structure entails researching various design alterations to widen the bandwidth of the structure and, thus, use the implementation of the EBG structure and spiral antenna more efficiently.

Initial research has been done into one of these alterations, cutting slits into the structure's patches. A patch design, referenced from [6], with four slits cut out of each patch has been initially implemented and tested to observe the effects on the design's band-gap characteristics. Figure 6.2.1 shows a comparison of the initial patch geometry for the EBG structure presented in this work to the patch geometry with slits cutout.

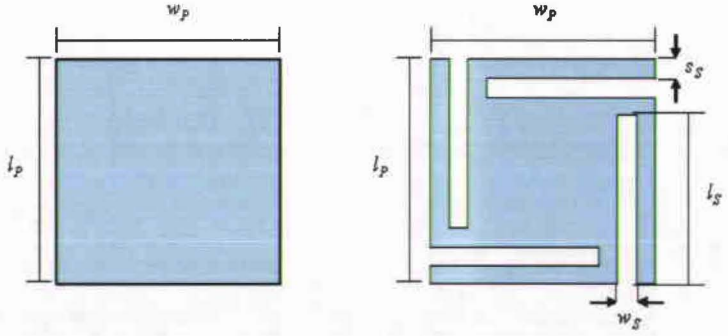

A. EBG Structure Patch **B. EBG Structure Patch with Slits**

Figure 6.2.1: EBG Structure Patch and EBG Structure Patch with Slits

According to [6] these slits should introduce multiple band-gaps, therefore, widening the effective range of the antenna. The parameters for the EBG structure remain the same as the design presented in this work, with: $l = w = 1.1\lambda$ (27.5mm), $l_P = w_P = 0.12\lambda$ (3mm), $s = 0.02\lambda$ (0.5mm), $d = 0.01\lambda$ (0.25mm), $t = 0.057\lambda$ (1.425mm), $h = 0.02\lambda$ (0.5mm), $\varepsilon_{r1} = 2.2$, and $\varepsilon_{r2} = 1$. The slits are designed with the following geometries: $l_S = 0.09\lambda$ (2.25mm), $w_S = 0.01\lambda$ (0.25mm), and $s_S = 0.01\lambda$ (0.25mm). Additionally, the Archimedean spiral's geometry has to be changed to include the higher frequency band-gap expected for the new patches with slits. This new geometry is designed for a frequency range of 8-30GHz and has the following geometries: $w_A = 0.016\lambda$ (0.4mm), $t_A = 0.004\lambda$ (0.1mm), $r_I = 0.5*(\lambda_H/2\pi)$ (0.75mm), and $r_O = 1.5*(\lambda_L/2\pi)$ (9mm). This new implementation can be seen in Figure 6.2.2.

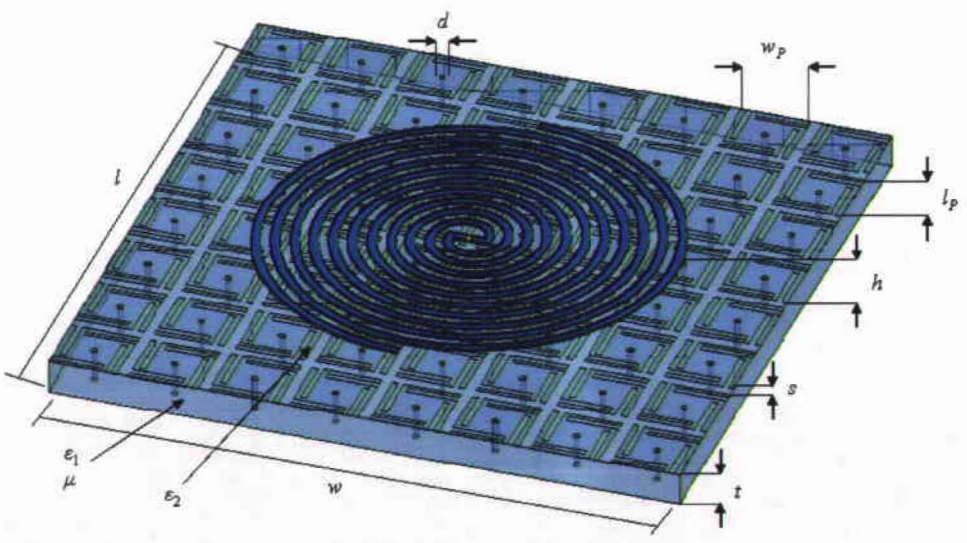

Figure 6.2.2: EBG Structure with Alternative Patch Geometry

Initial results from this design show the addition of a secondary band-gap at higher frequencies. Currently, further research is being done into the advantages of this alternative patch design.

Additionally, there are plans to explore other patch geometry alterations and their broadband characteristics. Other research directions include alternative EBG structure geometries, i.e., capactively loading the EBG structure by implementing multi-layers or inductively loading the structure by implementing coils or other techniques [5]. Additional future work includes in-depth analyses of the effects of the various geometries associated with the EBG structure and antenna design on antenna performance. Additionally, it is of interest to implement the designed EBG structure with other wide-band antennas. Ultimately, simulation observations will need experimental validation.

REFERENCES

1. W. Stutzman, G. Thiele, *Antenna Theory and Design*, John Wiley & Sons, Inc., 1998.
2. M. Afsar, Y. Wang, H. Ding, *A New Wideband Cavity-Backed Spiral Antenna*, Antennas and Propagation Society International Symposium, 2001, IEEE, vol. 4, pp. 124-127, July 2001.
3. R. Harrington, *Time-Harmonic Electromagnetic Fields*, McGraw-Hill, 1961.
4. J. Kraus, *Antennas*, McGraw-Hill, 1950.
5. D. Sievenpiper, *High-Impedance Electromagnetic Surfaces*, Ph.D. Dissertation, University of California, Los Angeles, 1999.
6. F. Yang, Y. Rahmat-Samii, *Reflection Phase Characterizations of the EBG Ground Plane for Low Profile Wire Antenna Applications*, IEEE Transactions on Antennas and Propagation, vol. 51, pp. 2691-2703, Oct. 2003.
7. J.J. Lee, S. Livingston, R. Koenig, *Wideband Long Slot Array Antennas*, Antennas and Propagation Society International Symposium, 2003, IEEE, vol. 2, pp. 452-455, June 2003.
8. D. Filipovic, J. Volakis, *Novel Slot Spiral Antenna Designs for Dual-Band/Multiband Operation*, IEEE Transactions on Antennas and Propagation, vol. 51, pp. 430-440, March 2003.
9. D. Filipovic, E. Siah, K. Sertel, V. Liepa, J. Volakis, *A Thin Broadband Cavity-Backed Slot Spiral Antenna for Automotive Applications*, Antennas and Propagation Society International Symposium, 2001, IEEE, vol. 1, pp. 414-417, July 2001.
10. Z. Li, Y. Rahmat-Samii, *PBG, PMC and PEC Ground Planes: A Case Study of Dipole Antennas*, Antennas and Propagation Society International Symposium, 2000, IEEE, vol. 2, pp. 674-677, July 2000.
11. M. Iskander, *Electromagnetic Fields and Waves*, Waveland Press, 1992.
12. E. Caswell, *Design and Analysis of Star Spiral with Application to Wideband Arrays with Variable Element Sizes*, Ph.D. Dissertation, Virginia Polytechnic Institute and State University, 2001.
13. J. Irwin, *Basic Engineering Circuit Analysis*, Macmillan Publishing, 1993.
14. B. Popovic, *Introductory Engineering Electromagnetics*, Addison-Wesley, 1971.
15. R. Collin, *Antennas and Radiowave Propagation*, McGraw-Hill, 1985.
16. P. Werntz, W. Stutzman, *Design, Analysis and Construction of An Archimedean Spiral Antenna and Feed Structure,* IEEE Proceedings of Souteastcon '89, 'Energy and Info Technologies in the Southeast', vol. 1, pp. 308-313, Apr. 1989.
17. J. Kaiser, *The Archimedean Two-Wire Spiral Antenna*, IEEE Transactions on Antennas and Propagation, vol. 8, pp. 312-323, May 1960.
18. C. Penney, R. Luebbers, *Input Impedance, Radiation Pattern, and Radar Cross Section of Spiral Antennas using FDTD*, IEEE Transactions on Antennas and Propagation, vol. 42, pp. 1328-1332, Sept. 1994.
19. T.H. Liu, W.X. Zhang, M. Zhang, K.F. Tsang, *Low Profile Spiral Antenna with PBG Substrate*, Electronics Letters, vol. 36, pp. 779-780, Apr. 2000.

20. Y. Qian, R. Coccioli, D. Sievenpiper, V. Radisic, E. Yablonovitch, T. Itoh, *A Microstrip Patch Antenna Using Novel Photonic Band-Gap Structures*, Microwave Journal, vol. 42, pp. 66-76, Jan. 1999.
21. T. Sudha, T.S. Vedavathy, *Microstrip Antennas and Arrays on Photonic Band Gap Substrates*, Proceedings of the 2001 SBMO/IEEE MTT-S International, vol. 1, pp. 105-108, Aug. 2001.